ISTITUTO NAZIONALE DI RICERCA METROLOGICA
Repository Istituzionale

Investigation of Verification Artifacts in WR-03 Waveguides

(Article begins on next page)

05 May 2024

Manuscript Number:	
Full Title:	Investigation of Verification Artifacts in WR-03 Waveguides
Article Type:	Devices
Keywords:	Scattering parameters; waveguide standards; measurement uncertainty; verification artifacts; microwave measurements
Corresponding Author:	Nosherwan Shoaib, Ph. D. Istituto Nazionale di Ricerca Metrologica Torino, Piemonte ITALY
Corresponding Author Secondary Information:	
Corresponding Author's Institution:	Istituto Nazionale di Ricerca Metrologica
Corresponding Author's Secondary Institution:	
First Author:	Nosherwan Shoaib, Ph. D.
First Author Secondary Information:	
Order of Authors:	Nosherwan Shoaib, Ph. D.
	Karsten Kuhlmann, Ph.D
	Rolf Judaschke, Ph.D
	Marco Sellone, Ph. D
	Luciano Brunetti, Ph.D
Order of Authors Secondary Information:	
Funding Information:	European Metrology Research Programme (EMRP) Project SIB62 Metrology for New Electrical Measurement Quantities in High-frequency Circuits (Project SIB62) — Karsten Kuhlmann
Abstract:	This paper presents an investigation of verification artifacts in WR-03 waveguides. The waveguide verification artifacts include a cross-guide and a custom-made circular iris section. The investigation involves the transmission loss uncertainty analysis of the verification artifacts for vector network analyzer (VNA) waveguide systems operating at millimeter wavelengths. The measurement errors due to the dimensional tolerances and the flange misalignment are predicted by using a commercially available electromagnetic software package. The data analysis is carried out for complex-valued scattering parameters (S-parameters). The uncertainty due to different error sources is computed according to the Law of Propagation of Uncertainty. The real and imaginary data along with the associated uncertainties are converted to magnitude and phase representation via linear propagation of uncertainties. The experimental results are also compared with simulated results.

Investigation of Verification Artifacts in WR-03 Waveguides

**Nosherwan Shoaib · Karsten Kuhlmann ·
Rolf Judaschke · Marco Sellone ·
Luciano Brunetti**

Abstract This paper presents an investigation of verification artifacts in WR-03 waveguides. The waveguide verification artifacts include a cross-guide and a custom-made circular iris section. The investigation involves the transmission loss uncertainty analysis of the verification artifacts for vector network analyzer (VNA) waveguide systems operating at millimeter wavelengths. The measurement errors due to the dimensional tolerances and the flange misalignment are predicted by using a commercially available electromagnetic software package. The data analysis is carried out for complex-valued scattering parameters (S-parameters). The uncertainty due to different error sources is computed according to the *Law of Propagation of Uncertainty*. The real and imaginary data along with the associated uncertainties are converted to magnitude and phase representation via linear propagation of uncertainties. The experimental results are also compared with simulated results.

Keywords Scattering parameters · waveguide standards · measurement uncertainty · verification artifacts · microwave measurements

1 Introduction

Network analysis of active and passive devices is a common task in RF & microwave engineering. It is usually carried out using vector network analyzers (VNAs). VNAs are complex and versatile instruments which are employed to characterize one-, two- or multi-port devices and provide the characterization

N. Shoaib · M. Sellone · L. Brunetti
Nanoscience and Materials Division, National Institute of Metrological Research (INRiM),
Strada delle cacce 91, Torino, ITALY
E-mail: nosherwan@live.com

K. Khulmann · R. Judaschke
High Frequency and Electromagnetic Fields, Physikalisch-Technische Bundesanstalt (PTB),
Bundesallee 100, 38116, Braunschweig, Germany

in terms of scattering parameters (S-parameters). The S-parameters of a device give information about its transmission and reflection properties [1].

Currently, VNA instrumentation is widely used for performing measurements at millimeter and sub-millimeter wavelengths. Beyond the mainframe upper operating frequency, waveguide extenders are used to further the measurement frequency range up to several hundreds of GHz [2]. In order to achieve reliability and accuracy of the measurements performed at such high frequencies, it is necessary to assess and verify the performance of the VNA systems. This is also important from the metrological point of view, to establish the traceability of the measurements to the International System of Units (SI). For the waveguide VNA setup, such verification is typically carried out at lower frequencies using precision and reduced height waveguide sections (shims). However, the dimensions of the waveguide sections become smaller with higher frequency waveguide bands. In particular, it is mechanically challenging to manufacture high precision waveguide sections with reduced height at higher millimeter and sub-millimeter frequencies because of very small dimensions of waveguide aperture. Currently, commercial verification artifacts for VNA measurements above 110 GHz are either not available or do not provide traceability to the SI.

Cross-guide devices have been introduced in the last couple of years as verification artifacts for measurements at frequencies above 110 GHz. The cross-guide device is a precision waveguide section which is connected in such a way that its aperture is rotated by 90 degrees with respect to rectangular waveguide aperture. These devices act as below-cutoff sections and provide significant transmission loss as verification standards [3]-[9]. Cross-guide devices can be used as calculable verification standards for different frequency bands depending on the dimensions of the waveguide aperture [8]. When using cross-guide devices, the pair of precision dowel holes are not usable anymore. However, these precision dowel holes can be used if the shim is specially fabricated for this purpose. Alternatively, a custom-made shim consisting of a circular iris section can be used since circular iris section is comparatively easier to realize. Such a custom-made circular iris section also provides comparable transmission losses when inserted between the rectangular waveguide test ports. Therefore, it can also be used as verification standard at millimeter and sub-millimeter frequencies [4], [9].

In this paper, the characterization of a WR-03 cross-guide and a custom-made circular iris section has been performed by taking into account the dimensional tolerances and the flange misalignment. The dimensional tolerances include the tolerances in the waveguide height, width, and length for the cross-guide and the tolerances in diameter and length for the circular iris section while the flange misalignment includes height, width and the connection angle. The measurement uncertainty due to dimensional tolerances and flange misalignment is computed based on the parametric information given in IEEE 1785.1-2012 standard [10] and in IEEE 1785.2-2014 standard [11]. The flange misalignment for cross-guide is derived from the specification for a UG-387 waveguide flange [12], while the flange misalignment for circular iris section is

derived from the values given in IEEE 1785.2-2014 standard [11]. The waveguide verification standards considered for analysis are a WR-03 cross-guide and a custom-made circular iris section. The frequency of interest ranges from 200 to 325 GHz.

The data analysis is carried out for real and imaginary parts of the S-parameter. The uncertainty due to different error sources is computed according to the *Law of Propagation of Uncertainty* [13], [14]. The real and imaginary data along with the associated uncertainty is converted to magnitude and phase representation via linear uncertainty propagation [14]. The electromagnetic computations are performed using a commercial simulation software package; Computer Simulation Technology (CST) Microwave Studio [15]. The experimental results are compared with the simulation results.

The paper is organized as follows: Sect. 2 discusses the electromagnetic modeling of the verification standards. Sect. 3 presents the mathematical formulations for the uncertainty evaluation. Results are presented and discussed in Sect. 4, followed by a conclusion.

2 Electromagnetic Simulations

The characteristics of the cross-guide and the circular iris section are computed using the time-domain solver of CST Microwave Studio. These characteristics are evaluated for the nominal values of dimensions of the artifact along with the dimensional tolerances as well as the flange misalignment. In the simulation model, the background material has been set to perfectly electrical conductor (PEC). Vacuum bricks are used to define the waveguide flange and the cross-guide connected between the two flanges. On the other hand, vacuum cylinders are used to define the circular iris section. The models illustrating the cross-guide and the circular iris section in CST Microwave Studio are shown in Fig. 1 and Fig. 2, respectively. The waveguide ports at the inputs of the waveguide flange sections are used for excitation. A hexahedral mesh is used for discretization. The S-parameters of the cross-guide and circular iris section without the feeding waveguide are obtained by de-embedding.

The transmission coefficient (S_{21}) of the cross-guide and the circular iris section is computed taking into account the parameter shown in Table 1. The corner radii of the waveguide aperture are assumed to have negligible influence on transmission loss computations, therefore, their influences are not taken into account.

CST Microwave Studio provides complex S-parameter data files for both the nominal values and the deviation of each parameter given in Tab. 1. Afterwards, the data is post processed with MATLAB [16]. All complex data along with uncertainty has been converted into magnitude and phase representation for graphical visualization. The detailed uncertainty evaluation procedure and the results are discussed in Sect. 3 and 4 respectively.
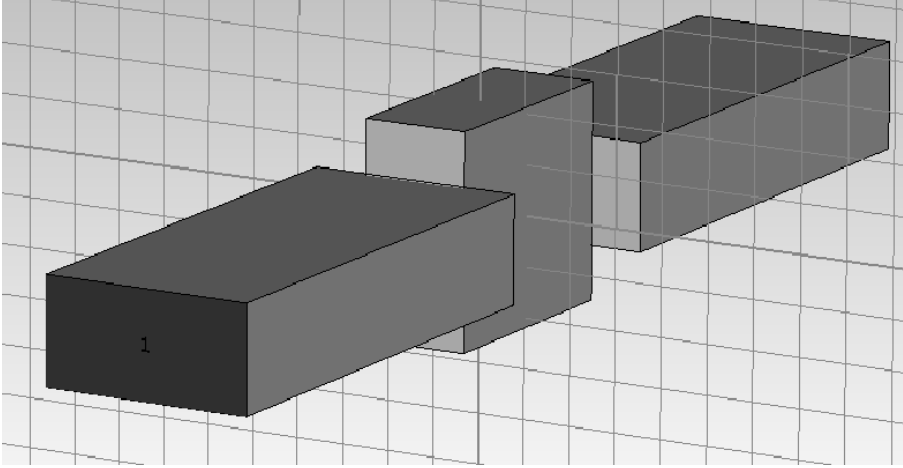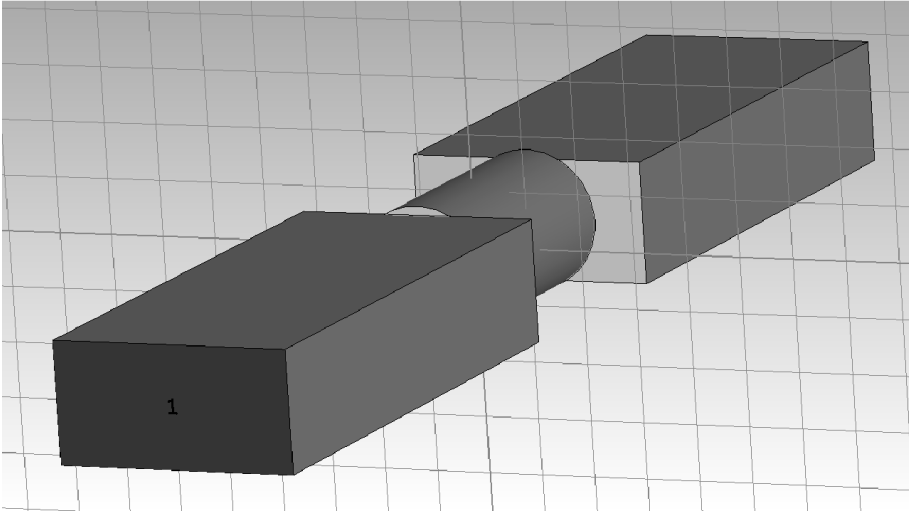
Fig. 1 Cross-guide connection strategy.

Fig. 2 Circular iris section connection strategy.

Table 1 Dimensional tolerances and flange misalignment for cross-guide and circular iris section.

Cross-Guide								
Nominal Width $a/$ μm	Nominal Height $b/$ μm	Length $l_w/$ μm	Dimensional Tolerances/μm			Flange Misalignments/μm		
			Width Δa_w	Height Δb_w	Length Δl_w	Width Δa_{fl}	Height Δb_{fl}	Connection Angle/^{o} $\Delta\Theta$
864	432	0.9830	4.3	4.3	3	150	150	1.2
Circular Iris Section								
Diameter $d_w/\mu m$			Diameter Δd_w					
499		0.9084	4.3		3	19	14	0.3

3 Uncertainty Evaluation

The transmission loss of the cross-guide and the circular iris section can be analyzed with respect to the uncertainty due to dimensional tolerances and flange misalignment shown in Tab. 1. The measurement uncertainty resulting from the different error sources has been computed according to the *Law of Propagation of Uncertainty* [13], [14]. The real and imaginary data along with the associated uncertainty have been converted in magnitude and phase representation via linear propagation of uncertainties [14].

Let us assume that the $S = x + jy$ denotes the complex-valued transmission S-parameter, where x and y represent the real and imaginary parts of the S-parameter respectively. The different sources of uncertainty are the dimensional tolerances and the flange misalignment shown in Tab. 1. For the cross-guide verification standard, the combined standard uncertainty for the real and imaginary part can be written in terms of dimensional tolerance and flange misalignment parameters shown in Tab. 1, as follows:

$$u(x) = \sqrt{ \underbrace{\left(\frac{\partial x}{\partial a_w}\right)^2 \left(\frac{\Delta a_w}{\sqrt{3}}\right)^2}_{(u_r(\Delta a_w))^2} + \underbrace{\left(\frac{\partial x}{\partial b_w}\right)^2 \left(\frac{\Delta b_w}{\sqrt{3}}\right)^2}_{(u_r(\Delta b_w))^2} + \underbrace{\left(\frac{\partial x}{\partial a_{fl}}\right)^2 \left(\frac{\Delta a_{fl}}{\sqrt{3}}\right)^2}_{(u_r(\Delta a_{fl}))^2} ... \\ + \underbrace{\left(\frac{\partial x}{\partial b_{fl}}\right)^2 \left(\frac{\Delta b_{fl}}{\sqrt{3}}\right)^2}_{(u_r(\Delta b_{fl}))^2} + \underbrace{\left(\frac{\partial x}{\partial \Theta}\right)^2 \left(\frac{\Delta \Theta}{\sqrt{3}}\right)^2}_{(u_r(\Delta \Theta))^2} + \underbrace{\left(\frac{\partial x}{\partial l_w}\right)^2 \left(\frac{\Delta l_w}{\sqrt{3}}\right)^2}_{(u_r(\Delta l_w))^2} , } \tag{1}$$

and

$$u(y) = \sqrt{ \underbrace{\left(\frac{\partial y}{\partial a_w}\right)^2 \left(\frac{\Delta a_w}{\sqrt{3}}\right)^2}_{(u_i(\Delta a_w))^2} + \underbrace{\left(\frac{\partial y}{\partial b_w}\right)^2 \left(\frac{\Delta b_w}{\sqrt{3}}\right)^2}_{(u_i(\Delta b_w))^2} + \underbrace{\left(\frac{\partial y}{\partial a_{fl}}\right)^2 \left(\frac{\Delta a_{fl}}{\sqrt{3}}\right)^2}_{(u_i(\Delta a_{fl}))^2} ... \\ + \underbrace{\left(\frac{\partial y}{\partial b_{fl}}\right)^2 \left(\frac{\Delta b_{fl}}{\sqrt{3}}\right)^2}_{(u_i(\Delta b_{fl}))^2} + \underbrace{\left(\frac{\partial y}{\partial \Theta}\right)^2 \left(\frac{\Delta \Theta}{\sqrt{3}}\right)^2}_{(u_i(\Delta \Theta))^2} + \underbrace{\left(\frac{\partial y}{\partial l_w}\right)^2 \left(\frac{\Delta l_w}{\sqrt{3}}\right)^2}_{(u_i(\Delta l_w))^2} , } \tag{2}$$

where, for example, $\left(\frac{\partial x}{\partial a_w}\right)$ is the sensitivity coefficient with respect to the (small) deviation in cross-guide width a_w. Δa_w is divided by a factor of $\sqrt{3}$ because it is assumed rectangular distribution. The parameter $u_r(\Delta a_w)$, represents the equivalent standard uncertainty due to a_w with respect to the real part of the S-parameter, while, $\left(\frac{\partial y}{\partial a_w}\right)$ is the sensitivity coefficient and describes how the imaginary part of S-parameter, y, varies with corresponding (small) deviation in cross-guide width a_w. The parameter, $u_i(\Delta a_w)$, represents the equivalent standard uncertainty due to a_w related to the imaginary part of the S-parameter. Accordingly, one can write the mathematical equations for circular iris section.

The expanded uncertainty has been computed by multiplying the standard uncertainty with coverage factor of 2. CST Microwave Studio has been used to obtain different transmission S-parameter data files for the nominal values and the deviation of each parameter given in Tab. 1. Afterwards, the different CST data files have been exported to MATLAB for post processing. A MATLAB script has been written based on Eqs. 1 and 2 to obtain different sensitivity coefficients and the uncertainty on real and imaginary parts of complex-valued S-parameter. The uncertainty on the real and imaginary part of the S-parameter have then been linearly propagated to obtain the magnitude and phase uncertainty.

4 Results and Discussions

In this section, the simulation and measurement results, showing the transmission loss magnitude and phase results along with combined expanded uncertainties, are presented. The expanded uncertainty has been computed using the coverage factor of 2. The uncertainty budgets containing the different error sources are presented as well.

The measurements were carried out under controlled ambient conditions at PTB using a two-port Rohde & Schwarz (R&S) ZVA-50 VNA equipped with two R&S ZVA-Z325 extenders operating up to 325 GHz. The VNA was calibrated using the Line-Reflect-Line (LRL) calibration algorithm [17]. The devices under test (DUTs) were a rectangular cross-guide and a custom-made circular iris sections. The custom-made circular iris section is also shown in Fig. 3.
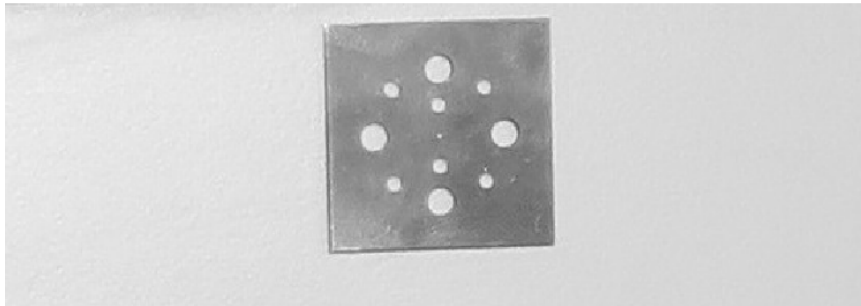

Fig. 3 Custom-made WR-03 circular iris section.

The measured transmission coefficient as function of frequency and the simulated values along with predicted uncertainty for the cross-guide and the circular iris are shown in Figs. 4 to 7. For both artifacts, the measured results given in magnitude and phase agree well with the simulated values. It can also be observed, that the cross-guide and the circular iris provide significant trans-

mission losses. Therefore, these artifacts can be used as verification standards to assess the attenuation (basis for linearity) of the VNA.
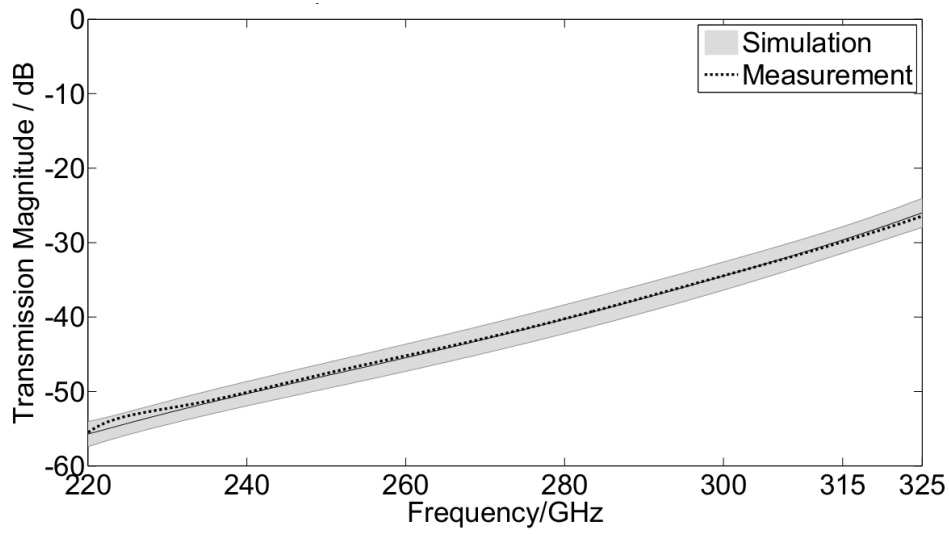

Fig. 4 Measurement and simulation of the transmission coefficient magnitude of the cross-guide.
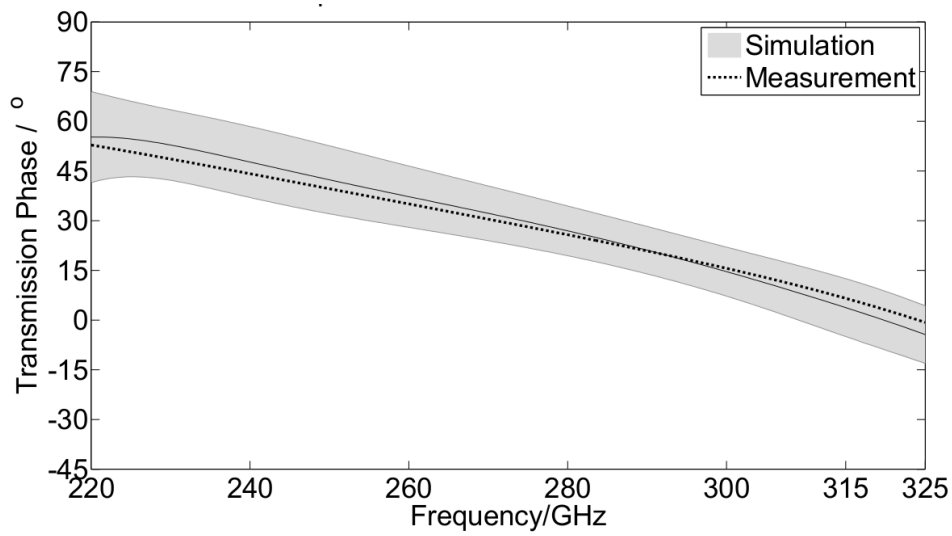
Fig. 5 Measurement and simulation of the transmission coefficient phase of the cross-guide.
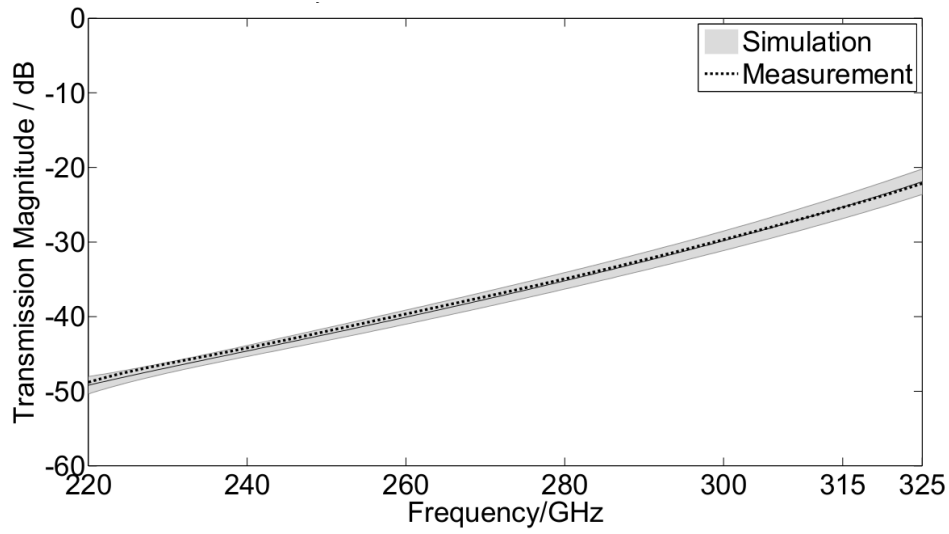
Fig. 6 Measurement and simulation of the transmission coefficient magnitude of the circular iris section.
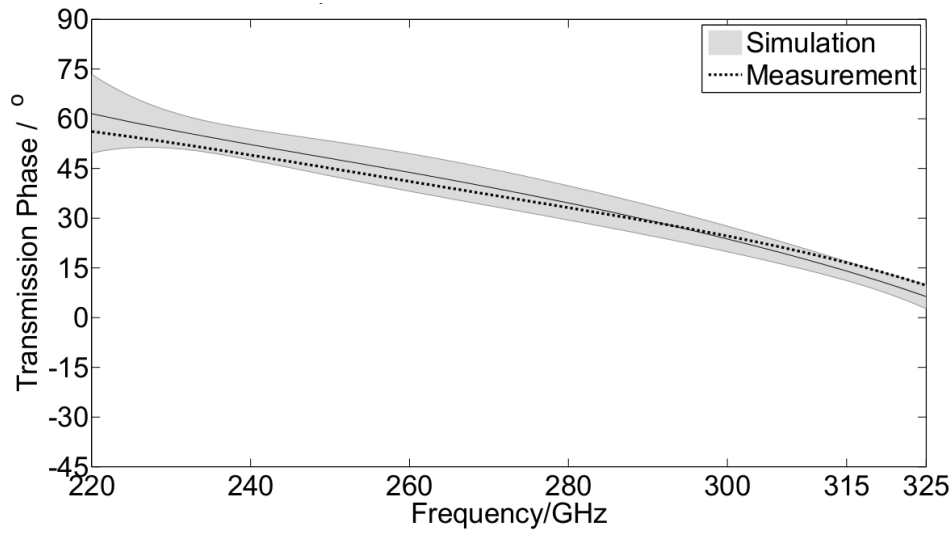

Fig. 7 Measurement and simulation of the transmission coefficient phase of the circular iris section.

The simulated transmission loss uncertainty budget tables 2 to 5 include the different uncertainty contributions for the real and imaginary part at se-

lected frequencies. The dimensional tolerances and the flange misalignment are the sources of uncertainties. The combined standard uncertainty (Std. Unc.) has been calculated as well.

Table 2 Uncertainty budget for the cross-guide at selected frequencies for the real part of the transmission coefficient. Std. Unc. represents the standard uncertainty.

Freq./ GHz	$Re(S_{21})$	Component Uncertainties						Std. Unc.
		$u(\Delta a_w)$	$u(\Delta b_w)$	$u(\Delta a_{fl})$	$u(\Delta b_{fl})$	$u(\Delta\Theta)$	$u(\Delta l_w)$	
220	0.00093	0.00001	0.00003	0.00023	0.00005	0.00002	0.00001	0.00024
250	0.00299	0.00001	0.00029	0.00041	0.00007	0.00005	0.00003	0.00051
280	0.00863	0.00002	0.00083	0.00083	0.00014	0.00019	0.00006	0.00120
310	0.02693	0.00006	0.00271	0.00077	0.00025	0.00016	0.00015	0.00284
325	0.04996	0.00012	0.00532	0.00167	0.00026	0.00069	0.00022	0.00563

Table 3 Uncertainty budget for the cross-guide at selected frequencies for the imaginary part of the transmission coefficient.

Freq./ GHz	$Im(S_{21})$	Component Uncertainties						Std. Unc.
		$u(\Delta a_w)$	$u(\Delta b_w)$	$u(\Delta a_{fl})$	$u(\Delta b_{fl})$	$u(\Delta\Theta)$	$u(\Delta l_w)$	
220	0.00135	0.00001	0.00006	0.00007	0.00003	0.00001	0.00001	0.00010
250	0.00272	0.00001	0.00016	0.00010	0.00002	0.00002	0.00002	0.00019
280	0.00438	0.00001	0.00019	0.00030	0.00001	0.00006	0.00003	0.00036
310	0.00356	0.00002	0.00053	0.00185	0.00015	0.00016	0.00002	0.00194
325	-0.00378	0.00001	0.00234	0.00285	0.00023	0.00088	0.00002	0.00380

Table 4 Uncertainty budget for the circular iris section at selected frequencies for the real part of the transmission coefficient.

Freq./ GHz	$Re(S_{21})$	Component Uncertainties					Std. Unc.
		$u(\Delta d_w)$	$u(\Delta a_{fl})$	$u(\Delta b_{fl})$	$u(\Delta\Theta)$	$u(\Delta l_w)$	
220	0.00166	0.00037	0.00014	0.00010	0.00003	0.00002	0.00041
250	0.00510	0.00039	0.00003	0.00001	0.00004	0.00004	0.00040
280	0.01431	0.00127	0.00001	0.00003	0.00011	0.00011	0.00128
310	0.04322	0.00398	0.00003	0.00010	0.00024	0.00026	0.00400
325	0.07970	0.00788	0.00021	0.00031	0.00033	0.00039	0.00790

Table 5 Uncertainty budget for the circular iris section at selected frequencies for the imaginary part of the transmission coefficient.

Freq./ GHz	$Im(S_{21})$	Component Uncertainties					Std. Unc.
		$u(\Delta d_w)$	$u(\Delta a_{fl})$	$u(\Delta b_{fl})$	$u(\Delta \Theta)$	$u(\Delta l_w)$	
220	0.00305	0.00013	0.00003	0.00001	0.00001	0.00003	0.00014
250	0.00566	0.00032	0.00001	0.00001	0.00001	0.00005	0.00032
280	0.00987	0.00042	0.00001	0.00001	0.00007	0.00007	0.00043
310	0.01360	0.00004	0.00005	0.00001	0.00031	0.00008	0.00033
325	0.00889	0.00224	0.00007	0.00015	0.00069	0.00004	0.00235

From the different uncertainty sources shown in Tab. 2 and 3 it can be observed, that the cross-guide aperture height (b_w) and the flange aperture width (a_{fl}) have the most significant influence on the transmission coefficient. On the other hand, the aperture width (a_w) and the length (l_w) have the least influence.

For the circular iris section, the uncertainty budget is presented in Table 4 and 5. The circular iris diameter (d_w) has the most significant influence on the real and imaginary part of the transmission coefficient, while the flange aperture width (a_{fl}) and height (b_{fl}) have the least influence on the real part and the flange aperture height (b_{fl}) has also the least influence on the imaginary part of the transmission coefficient.

The simulated results and uncertainties are presented in Tab. 6 and 7.

Table 6 Magnitude and phase values of the transmission coefficient for the cross-guide at selected frequencies.

Freq./ GHz	$S_{21}/$ dB	$S_{21}/^o$	Std. Unc./dB	Std. Unc./^{o}
220	-55.71	55.22	0.85	6.87
250	-47.87	42.34	0.87	5.13
280	-40.29	26.94	0.97	3.75
310	-31.32	7.54	0.90	4.16
325	-26.00	-4.33	0.98	4.35

Table 7 Magnitude and phase values of the transmission coefficient for the circular iris section at selected frequencies.

Freq./ GHz	$S_{21}/$ dB	$S_{21}/^o$	Std. Unc./dB	Std. Unc./^{o}
220	-49.19	61.51	0.59	5.94
250	-42.36	48.03	0.43	2.63
280	-35.20	34.59	0.55	2.58
310	-26.88	17.47	0.73	1.57
325	-21.92	6.37	0.85	1.83

5 Conclusion

This paper analyzes the transmission loss magnitude and phase uncertainty of waveguide artifacts to be used for attenuation measurements. The verification artifacts are a WR-03 cross-guide and a custom-made circular iris section. The effects on the transmission magnitude and phase of the verification artifacts due to dimensional tolerances and flange misalignment have been predicted using CST Microwave Studio. The model-based measurement uncertainty due to different error sources is computed according to the *Law of Propagation of Uncertainty*. The measured values are in a good agreement with the simulated values within the model-based uncertainty intervals. It is concluded that the circular iris section can be used as an alternative to cross-guide to assess the performance of VNAs operating at millimeter wave frequencies.

The future extension of this work would be to estimate the complete measurement uncertainty for traceable VNA measurements. The uncertainty would further be included by the calibration standards, VNA noise, repeatability and drift.

References

1. M. Hiebel, Fundamentals of Vector Network Analysis, 3rd edition, Chap. 1, Rohde & Schwarz GmbH & Co., Germany (2008)
2. D. Adamson, N. M. Ridler, J. Howes, Recent and Future Developments in millimeter and Sub-millimeter Wavelength Measurement Standards at NPL, 5th ESA Workshop on millimeter Wave Technology and Applications & 31st ESA Antenna Workshop, 463-467, Netherlands (2009)
3. N. M. Ridler, R. G. Clarke, M. J. Salter, A. Wilson, Traceability to national standards for S-parameter measurements in waveguide at frequencies from 140 GHz to 220 GHz, Proc. 76th ARFTG Microwave Measurement Conference, 1-7, Clearwater Beach, FL (2010)
4. T. Schrader, K. Kuhlmann, R. Dickhoff, J. Dittmer, M. Hiebel, Verification of scattering parameter measurements in waveguides up to 325 GHz including highly-reflective devices, Advances in Radio Science, 9, 917 (2011)

5. N. M. Ridler, M. J. Salter, Cross-connected waveguide lines as standards for millimeter- and submillimeter-wave vector network analyzers, 81st ARFTG Microwave Measurement Conference (ARFTG), 1-7, Seattle, Washington, USA (2013)

6. N. M. Ridler, R. Clarke, M. J. Salter, A. Wilson, The Trace Is on Measurements: Developing Traceability for S-Parameter Measurements at Millimeter and Submillimeter Wavelengths, IEEE Microwave Magazine, 14, 67-74 (2013)

7. H. Huang, N. M. Ridler, M. J. Salter, Using electromagnetic modeling to evaluate uncertainty in a millimeter-wave cross-guide verification standard, 83rd ARFTG Microwave Measurement Conference (ARFTG), 1-5, Tampa, Florida, USA (2014)

8. M. J. Salter, N. M. Ridler, Use of reduced aperture waveguide as a calculable standard for the verification of millimeter-wave vector network analyzers, Proc. 44th European Microwave Conference, 750-753, Rome, Italy (2014)

9. N. Shoaib, K. Kuhlmann, R. Judaschke, Investigation of verification artefacts in rectangular waveguides up to 325 GHz, 1st URSI Atlantic Radio Science Conference (URSI AT-RASC), Gran Canaria, Spain (2015)

10. IEEE Standard 1785.1-2012, IEEE P1785: IEEE Standard for Rectangular Metallic waveguides and Their Interfaces for Frequencies of 110 GHz and Above - Part 1: Frequency Bands and Waveguide Dimensions (2012)

11. IEEE Standard 1785.2-2014, IEEE P1785.2: Draft Standard for Rectangular Metallic waveguides and Their Interfaces for Frequencies of 110 GHz and Above, IEEE standards draft (2015)

12. MIL-DTL-3922/67D, Flanges, Waveguide (Contact) (Round, 4 hole) (Millimeter) (2009)

13. John R. Taylor, An Introduction to Error Analysis, The Study of Uncertainties in Physical Measurements. 2nd edition, 209-914, Sausalito, CA: University Science Books (1982)

14. BIPM, IEC, IFCC, ILAC, ISO, IUPAC, IUPAP and OIML, JCGM 100:2008, evaluation of measurement data - Guide to the expression of uncertainty in measurement, International Organization for Standardization (ISO) (2008) [Online]. Available: `http://www.bipm.org/en/publications/guides/gum.html`

15. CST - Computer Simulation Technology (2014)
    Information available at: `http://www.cst.com`

16. MATLAB - The Language of Technical Computing (2011)
    Information available at: `http://www.mathworks.com`

17. N. Ridler, Choosing line lengths for calibrating waveguide vector network analyzers at millimeter and sub-millimeter wavelengths, NPL Report TQE 5, 121 (2009)